Opening and Closing Motions in the Periplasmic Vitamin B_{12} Binding Protein BtuF†

Christian Kandt, Zhitao Xu, and D. Peter Tieleman*

Department of Biological Sciences, University of Calgary, 2500 University Drive NW, Calgary, Alberta T2N 1N4, Canada

Received June 26, 2006; Revised Manuscript Received August 28, 2006

ABSTRACT: BtuF is the periplasmic binding protein (PBP) in the vitamin B_{12} uptake system in *Escherichia coli* where it is associated with the ABC transporter BtuCD. When the ligand binds, PBPs generally display large conformational changes, commonly termed the Venus flytrap mechanism. BtuF belongs to a group of PBPs that, on the basis of crystal structures, does not appear to display such behavior. Using 480 ns multicopy molecular dynamics simulations of apo and holo forms of the protein, we investigate the dynamics of BtuF. We find BtuF to be more flexible than previously assumed, displaying clear opening and closing motions which are more pronounced in the apo form. The protein behavior is compatible with a PBP functional model that postulates a closed conformation for the ligand-bound state, whereas the empty form fluctuates between open and closed conformations. Elastic network normal-mode analysis suggests that all BtuF-like PBPs are capable of similar opening and closing motions. It also makes the typical Venus flytrap domain motions a likely common means of how PBP−ABC transporter interaction could occur.

Periplasmic binding proteins (PBPs) are found between the inner and outer membrane of Gram-negative bacteria where they mediate solute transport or initiate chemotaxis by activating flagellar motion (*1*−*4*). PBPs bind a broad palette of substrates ranging from sugars, amino acids, and peptides to a variety of ion compounds and vitamins (*3*). There is also some evidence that PBPs might be involved as chaperones in the refolding of denatured proteins (*5*). Having only one membrane, Gram-positive bacteria employ similar but membrane-anchored versions of PBPs (*6*, *7*) to acquire nutrients from their environment. Furthermore, many eukaryotic receptors contain extracellular ligand binding domains which are homologous to PBPs (*3*).

The large spectrum of substrates recognized by PBPs is reflected in a large gene family encoding many binding proteins with rather diverse sequences (*3*). Despite diversity in primary structure, PBPs share a common structural motif of two globular domains connected by a variably organized linker region. Ligand binding takes place in a cleft between the two lobes and generally induces a large conformational change during the course of which the domains close around the bound substrate. This is commonly termed the "Venus flytrap" motif (*8*). To explain the PBP working mechanism, two functional models have been proposed, both characterized by an equilibrium between empty and ligand-loaded forms of the protein. According to the first model, which was first introduced on the basis of small-angle X-ray scattering data and computer modeling results for the arabinose PBP (*9*), the empty form of the protein exists in a stable open conformation and ligand binding triggers a transition toward an equally stable closed state. The second model is based on X-ray crystallographic results first described for the lysine-arginines-ornithine binding protein and proposes that the empty form of the protein exists in a dynamic equilibrium between open and closed states, whereas when the ligand binds, the protein exhibits only the closed conformation (*10*).

PBPs can be classified on the basis of similarities in primary sequence (*1*, *11*) or by the topology of their globular domains (*12*−*14*) in terms of the arrangement of secondary structure elements. An alternative classification is based on the number of interdomain connections. Three groups have been identified so far, and they are characterized by either one (group III), two (group II), or three (group I) interdomain connections (*2*, *15*). To date, more than 100 X-ray structures of PBPs and related binding proteins have been determined from a variety of organisms, including eubacteria, archaea, and eukaryotes (*4*). Remarkably, only X-ray structures of group I or II PBPs appear to exhibit large conformational changes between empty and ligand-bound states, with the group I maltose binding protein being a prominent and widely studied example (*16*). In contrast, group III PBPs, with their lobes connected by only a single α-helix, appear to undergo no comparable conformational changes upon substrate binding. The structures of four group III PBPs have been determined by X-ray crystallography: zinc binding protein TroA (*17*, *18*), surface manganese binding protein PsaA (*19*), ferrochrome binding protein FhuD (*20*, *21*), and vitamin B_{12} binding protein BtuF (*15*, *22*). Crystal structures of TroA, FhuD, and BtuF of both empty and ligand-bound states are available.

BtuF is the periplasmic binding protein in the Btu (B_{12} uptake) system in *Escherichia coli* (*23*), which to date is the only import system with crystal structures of all its key components available. These components include TonB-

† This work is supported by the Canadian Institutes of Health Research. C.K. and Z.X. are postdoctoral fellows of the Alberta Heritage Foundation for Medical Research. D.P.T. is an AHFMR Senior Scholar and CIHR New Investigator.

* To whom correspondence should be addressed. E-mail: tieleman@ucalgary.ca. Fax: (403) 289-9311. Phone: (403) 220-2966.

10.1021/bi061280j CCC: $33.50
Published on Web 10/13/2006

dependent transporter protein BtuB (*24*), which transfers vitamin B_{12} across the outer membrane, and ABC transporter BtuCD (*25*) in the inner membrane. ABC transporters form a large class of proteins occurring in all forms of life (*26*). They are involved in multidrug resistance in cancer and in a number of human genetic diseases. Crystal structures are available for only two full ABC transporters: one is the lipid flippase MsbA (*27*−*29*), and the other is the vitamin B_{12} importer BtuCD (*25*), to which BtuF delivers the cyanocobalamin after binding it in the periplasmic inter-membrane space. Once docking occurs, a stable BtuCD-F complex is formed, and transport across the inner membrane is initiated (*30*). A likely docking interface has been proposed (*15*), and the BtuCD-F complex was successfully reconstituted in lipid vesicles where it was functionally characterized (*31*). However, both the structure of the BtuCD-F complex and the functional details of the transport process are still unknown.

Against this background, we want to address the question of the BtuF function mechanism. Does BtuF fit into one of the two existing functional models for PBPs, or does it represent a new group? Are there only minor conformational differences between the empty and loaded state, as the X-ray structures suggest, or could this be a limitation imposed by the crystallization procedures? For other ABC transporter-associated PBPs like maltose binding protein, the large conformational changes upon ligand binding suggest a clear means of distinguishing between empty and loaded PBPs and also a possible way of PBP and ABC transporter interaction and communication. If the Venus flytrap mechanism applies to BtuF as well, this could hint at a more general scheme of PBP−ABC transporter interaction, which would be particularly interesting because the crystal structure of the ABC transporter BtuCD is known. Thus, the dynamics of BtuF may be of more general interest in understanding the mechanism of ABC transporters.

To this purpose, we used multicopy molecular dynamics (MD) simulations (*32*, *33*) to explore the conformational space accessible to BtuF. Four MD studies on periplasmic binding proteins have been reported so far. Simulations of the glutamine binding protein (*34*), the PBP homologue ligand binding domain of glutamate receptor GluR2 (*35*), and the maltose binding protein (*36*) focused on the transition between the open and closed state, whereas a simulation study of ferrochrome binding protein FhuD explored the conformational space accessible to an apo form of the protein created by removing the bound ligand (*37*). In our study, we consider BtuF in both the ligand-free and ligand-bound forms, each of which is additionally characterized in a ligand-added and ligand-removed state. We also performed elastic network normal-mode analysis (refs *38* and *39* and references cited therein) of BtuF and all BtuF-like (group III) periplasmic binding proteins to gain insight into structure-inherent and possibly functionally relevant conformational changes characterized by the proteins' lowest-frequency normal modes. Elastic network normal-mode analysis has been successfully applied to crystal structures and electron microscopy data in predicting conformational changes in proteins such as membrane channel opening (*40*) or ribosomal movements (*41*, *42*).

We find BtuF to be more flexible than previously assumed, displaying clear opening and closing motions which are more pronounced in the apo form. This protein behavior is compatible with the second PBP functional model. Elastic network normal-mode analysis suggests that all group III PBPs are capable of similar opening and closing motions.

EXPERIMENTAL PROCEDURES

Simulation Systems. Molecular dynamics simulations were performed using GROMACS 3.2.1 and the ffgmx force field (*43*, *44*). The 1N4D (3.0 Å resolution, ligand-free) and 1N4A (2.0 Å resolution, ligand bound) BtuF crystal structures (*22*) were used as starting structures. Four different simulation systems were created: two featuring the unmodified apo and holo X-ray structures and two containing modified ones where the cobalamin ligand had been removed in one case and added in the other. In every case, the protein was then inserted into a truncated octahedral box and solvated with ∼15000 simple point charge water molecules (*45*). One chloride ion was added to neutralize the system's net charge. Standard protonation states were assumed for titratable residues.

Multicopy MD simulations (*32*, *33*) were performed; for each system, three production runs were initiated using a different temperature seed to generate the random distribution of starting velocities. The simulations were started with the protein and vitamin B_{12} position-restrained. A force constant of 1000 kJ mol^{-1} nm^{-2} was applied during the first 10 ps of the simulation, and in course of the following 20 ps, force constants were lowered to 10 kJ mol^{-1} nm^{-2}. After that point, no position restraints were applied and production runs began. Twelve individual production runs were performed, with simulation times ranging from 30 to 50 ns, yielding a total simulation time of 480 ns (Figure 1).

In the simulations, all bond lengths were constrained so that an integration time step of 2 fs could be used for LINCS (65). Systems were simulated at a temperature of 310 K, maintained separately for water and protein by a Berendsen thermostat (*46*) with a time constant of 0.1 ps. A Berendsen barostat (*46*) was used with isotropic pressure coupling with a time constant of 1 ps and a reference pressure of 1 bar. Electrostatic interactions were calculated using particle mesh Ewald summation (*47*, *48*), and twin range cutoffs of 0.9 and 1.4 Å were applied in computing the van der Waals interactions.

Vitamin B_{12} Force Field Parameters. A vitamin B_{12} topology was developed for the GROMACS ffgmx force field, starting from AMBER cyanocobalamin parameters as a template (*49*). Due to inconsistencies in that topology, such as the negatively charged cobalt and numerous redundant dihedral definitions each with a force constant of zero, a simple conversion of the parameter set was not possible. Instead, a different strategy was followed. For the cobalt, van der Waals ϵ and σ parameters were taken from a corrinoid topology for the MM2 force field (*50*) from which the AMBER topology had originally been derived; elsewhere, GROMACS atom types were assigned. Once atom types are defined, parameters describing bonded interactions can be derived from connectivity patterns. Additionally, vitamin B_{12} could be subdivided into parts already available in the ffgmx force field. For example, the corrinoid ring contains glutamine-like ligands, while the lipid-like phosphate group, sugar, and heterocycle group all resemble parts of NADH or FADH. For each part of vitamin B_{12} (Figure 2A) thus described, their

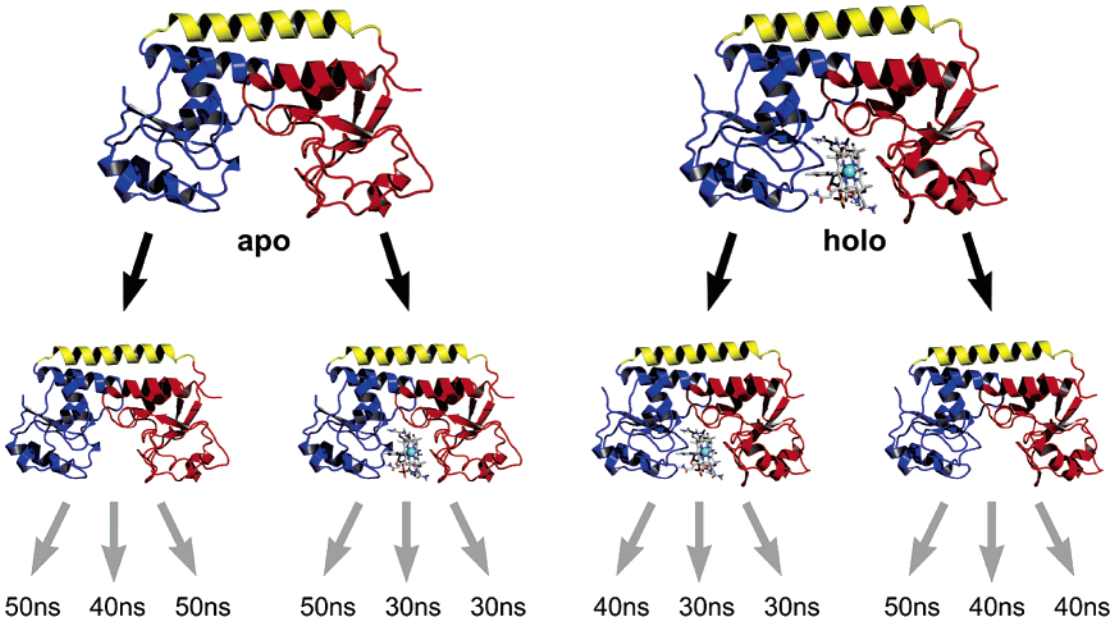

FIGURE 1: Four different simulation systems generated on the basis of the apo and holo BtuF crystal structures. From left to right are the unmodified apo X-ray structure (no-B_{12}), the modified apo model with added ligand (B_{12}-added), the unmodified holo crystal structure (B_{12}-bound), and the modified holo structure with the ligand removed (B_{12}-removed). For each system, three multicopy MD simulations were performed using a different random distribution of starting velocities. BtuF is colored according to its main structural components: N- and C-terminal domains colored blue and red, respectively, with the domain connection α-helix colored yellow.

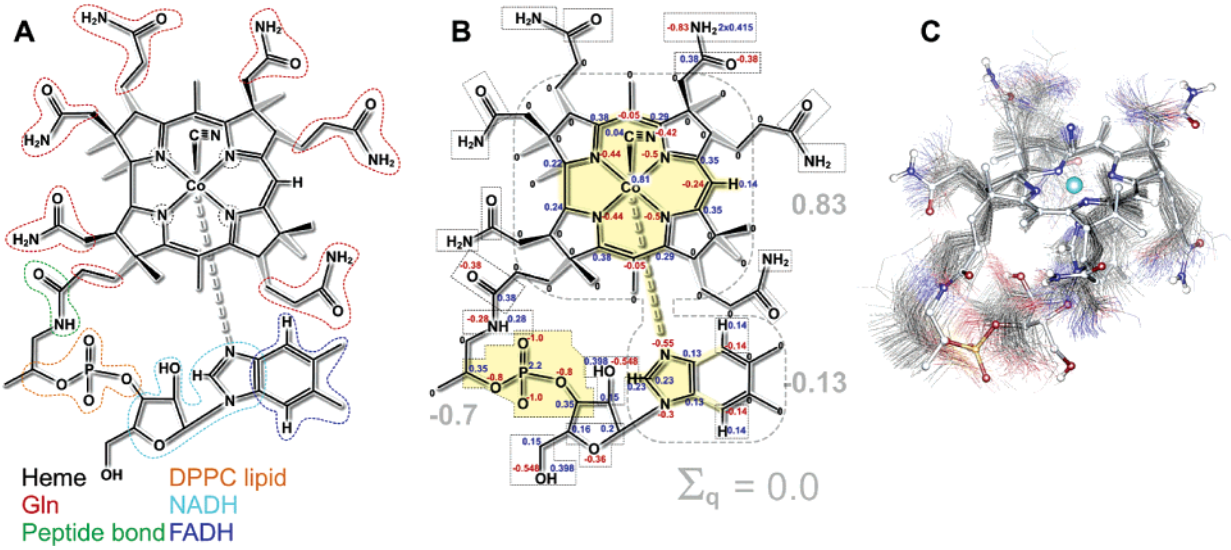

FIGURE 2: We developed vitamin B_{12} force field parameters for the ffgmx GroMACS force field. Segments of vitamin B_{12} resemble molecule parts for which GroMACS parameters are already available (A). Charge groups (boxes) and partial charges either come from molecule segments already known to GroMACS or are based on quantum mechanical (QM) calculations. QM parts are highlighted in yellow. The gray dotted line frames atoms among which no nonbonded interactions have been calculated (B). As reflected by snapshots (wireframe) from a 1 ns MD simulation in water that have been superimposed on the vitamin B_{12} X-ray structure (ball and stick), our topology yields a stable description of cyanocobalamin (C).

bonded and nonbonded ffgmx interaction parameters were adopted.

Additionally, quantum mechanical calculations using GAUSSIAN 03 (*51*) were carried out to investigate the detailed charge distribution. This was done for both the whole molecule and a core section of vitamin B_{12} consisting of the corrinoid ring π-electron system and the five-body part of the heterocycle liganding the cobalt. Adjacent carbons were included as methyl groups. Geometries of both versions of vitamin B_{12} were optimized at the HF level with the STO-3G basis set, followed by a single-point calculation at the B3LYP (*52*, *53*) level of density functional theory (DFT) using the Lanl2dz basis set (*54*) and pseudopotential for the cobalt atom and 6-31G** basis sets for the other atoms. Natural population analysis (NPA) (*55*) was used to estimate the atomic charges from the electron densities. These all-atom charges were then summed and averaged to fit the united-atom nature of the ffgmx force field. The only difference in partial charges derived from the full and partial QM approach was found in sections directly adopted from the ffgmx force field, mainly the amino groups of the glutamine-like ligands. Therefore, part QM/part ffgmx

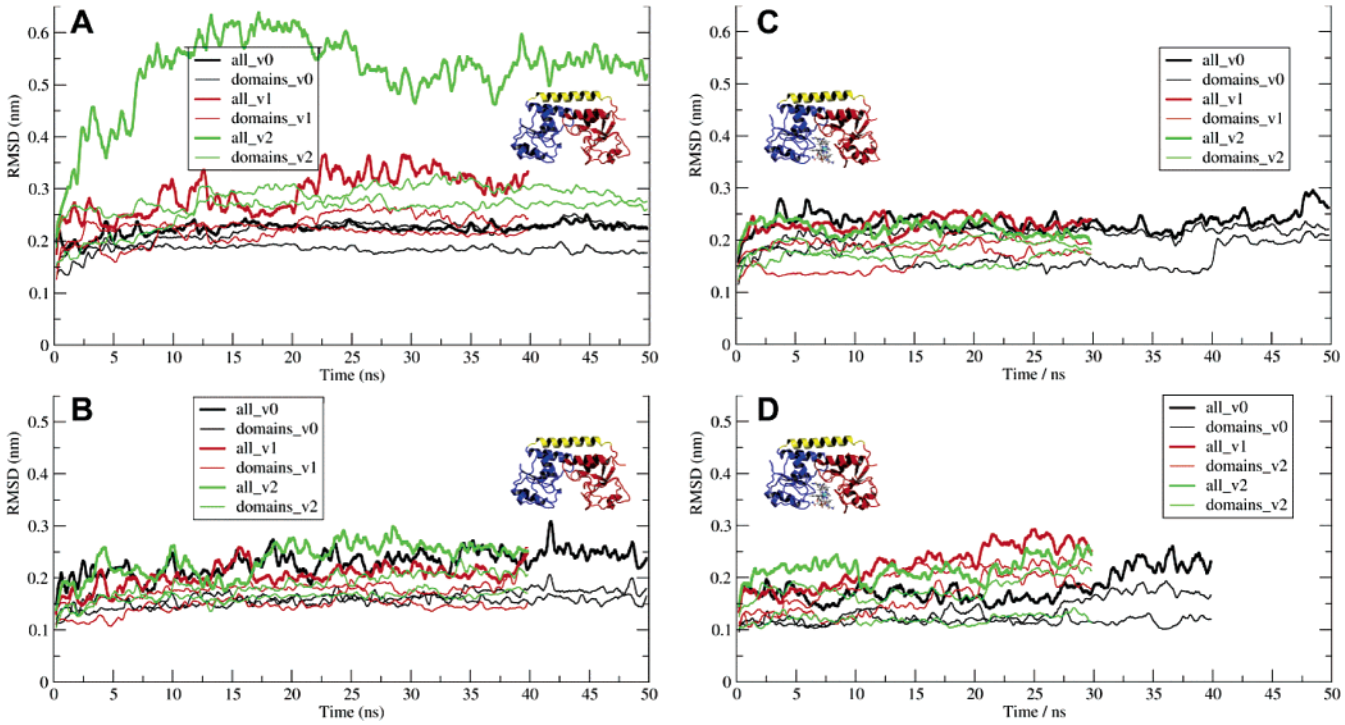

FIGURE 3: C_α rmsd plots for the four different BtuF simulation systems and the three copies of each: no-B_{12} (A), B_{12}-removed (B), B_{12}-added (C), and B_{12}-bound (D). The rmsds of N- and C-terminal domains are always smaller than the corresponding rmsd of the whole protein.

charges were used for simulations to yield a greater consistency with the ffgmx force field. To stabilize ring geometry, nonbonded interactions are not computed among atoms of the corrinoid ring or the N-heterocycle. Partial charges and applied exclusions are summarized in Figure 2B.

As an initial test, vitamin B_{12} was solvated, and 1 ns of unrestrained MD was performed, implementing the protein run simulation settings. As indicated by simulation snapshots superimposed on the X-ray structure (Figure 2C), our topology appears to yield a stable description of vitamin B_{12} for MD simulations, with flexible regions as expected.

Elastic Network Normal-Mode Analysis. To detect functionally relevant large-scale movements in BtuF and BtuF-like periplasmic binding proteins, elastic network normal-mode analysis was performed using the NOMAD-Ref server (*38*). The first five lowest-frequency modes were calculated using the server's standard settings: all heavy atoms included, a 5 Å distance weight parameter, and a 10 Å distance cutoff used for mode calculation. Only atom pairs closer than the distance cutoff are linked by Hookean springs, whereas the distance weight parameter is applied in the calculation of pair interactions to yield a smoother cutoff. Where possible, the proteins were considered in their open conformation. The protein X-ray structures that were analyzed include apo BtuF (1N4D) (*22*), gallichrome-bound FhuD (1EFD) (*20*) [at present, the apo FhuD structure (*21*) is not yet available from the Protein Data Bank], TroA in the zinc-bound open conformation (1TOA) (*17*), and zinc-bound PsaA (1PSZ) (*19*).

Domain Motion Analysis. On the basis of the apo and holo BtuF extreme conformations depicted in panels C and D of Figure 4, a domain motion analysis was carried out using the DynDom web server at http://www.cmp.uea.ac.uk/dyndom/ (*56*−*58*). Standard settings were used.

RESULTS

Conformational Changes. Structural changes in BtuF occurring throughout the simulations were monitored by C_α root-mean-square deviations computed for each run with respect to their corresponding starting structure (Figure 3) and C_α distance changes calculated between conserved glutamates 50 and 180 (Figure 4), which have been proposed to be key residues in the BtuF−BtuC docking interface (*15*).

Root-mean-square deviation (rmsd) plots in Figure 3 are presented separately for each of the four starting structures: no-B_{12} and B_{12}-removed (apo BtuF, Figure 3A) and B_{12}-added and B_{12}-bound (holo BtuF, Figure 3B). Each panel holds nine graphs representing the C_α rmsds of the full protein and its N- and C-terminal domains (residues 1−105 and 130−244). Three main observations are made. (1) Different copies of the same simulations with different starting velocities yield different conformational changes as reflected by different rmsds. (2) The rmsds of the individual N- and C-terminal domains are always smaller than the rmsd of the whole protein. (3) The maximum rmsds for the whole protein range between 1.6 and 2.6 Å, except for copy 2 of the unmodified no-B_{12} X-ray structure, for which the maximum rmsd is 6.3 Å. At the same time, the rmsds of N- and C-terminal domains do not exceed 3 Å.

Glu50−Glu180 C_α distance plots in Figure 4 are given separately for the apo and holo runs of BtuF, each holding the results for unmodified (no-B_{12} and B_{12}-bound) and modified X-ray starting structures (B_{12}-added and B_{12}-removed). In the apo simulations, the Glu50−Glu180 C_α distance increases during four runs, decreases in one run, and reverts to the starting distance after an initial increase of 2 Å in the remaining sixth run (Figure 4A). In the holo simulations, the distance between the two conserved glutamates increases during one run and decreases during three runs.

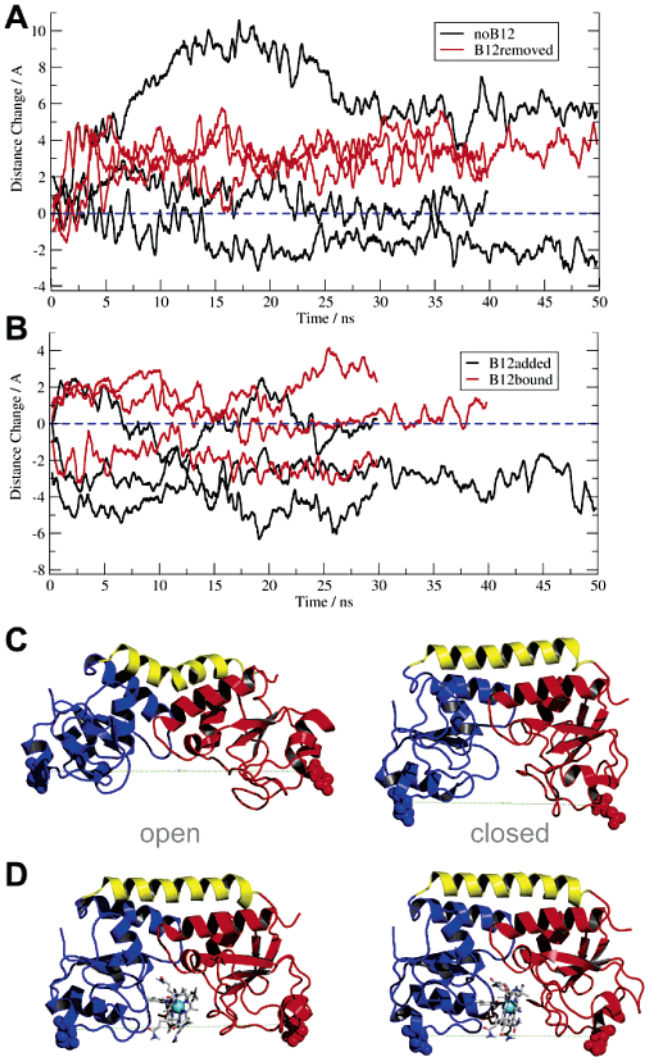

FIGURE 4: Opening and closing motions of BtuF as reflected by the change in the C_α distance between conserved glutamates 50 and 180 (A and B). The extreme conformations are based on minima and maxima in the Glu distance graph. Both apo (C) and holo (D) forms display opening and closing motions, but the conformational changes in the apo form are larger.

Of the remaining two cases, in one the distance change reverts to 0 Å after an increase of 2 Å. In the second, the Glu C_α distance fluctuates around its starting length with an amplitude of 2 Å (Figure 4B). The largest distance changes constitute an increase of 10 Å and a decrease of 2.5 Å in the apo simulations, while in the holo runs, a maximum increase of 4 Å and a decrease of 6.2 Å are observed. Runs starting from the unmodified no-B_{12} X-ray structure exhibit both increases and decreases in the Glu50−Glu180 C_α distance. In all B_{12}-removed simulations, the distance decreases. In the holo BtuF simulations, both an increase and a decrease in glutamate distance are observed for the B_{12}-bound runs, but no increase is detected for the B_{12}-added runs. BtuF conformations corresponding to minimum and maximum values of the Glu50−Glu180 C_α distance reveal opening- and closing-like motions of the N- and C-terminal domains in both the apo and holo form of the protein, with larger motions in the apo form (Figure 4C,D). The maximum distance increase of 10 Å in the apo no-B_{12} copy 2 simulation is due to a wide opening motion of the domains, accompanied by a kink of the α-helix connecting the two domains: at

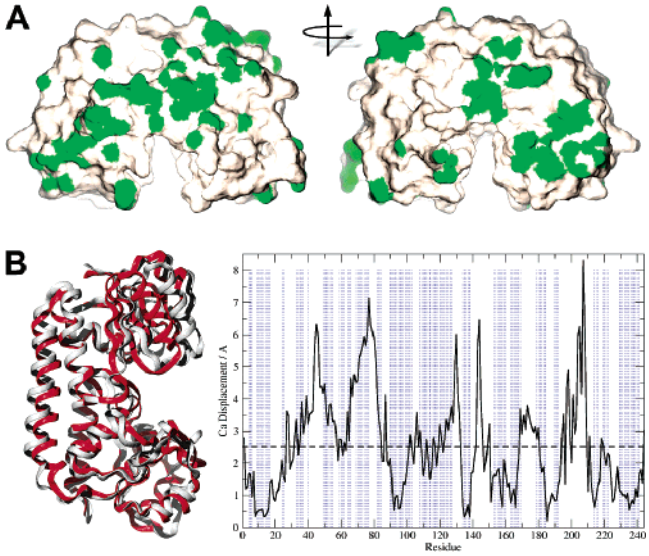

FIGURE 5: In the X-ray structural models, no opening or closing motions are observed. Crystal contacts (green) might hinder an opening of BtuF (A), or the open conformation could be part of the BtuF crystal; however, the majority of the conformation is in the closed state. When the average structure from all no-B_{12} runs (red) is computed and superimposed on the apo crystal structure (white), the difference between the two is small (B). Larger deviations occur mainly in the loop regions (α-helix and *β*-sheet components are highlighted in blue in the C_α displacement plot), and the overall rmsd is 2.5 Å (dashed line).

Ser116, the regular α-helical $n-n+4$ backbone hydrogen bonding pattern is broken when its backbone oxygen is tilted outward. In this scenario, either Gln115 forms backbone hydrogen bonds to both Asp119 and Gln120 or the side chain of Gln120 folds back and H-bonds with its own carbonyl oxygen, which in turn brings its amino group into possible interaction distance of the Ser116 backbone oxygen. The helix kink is not observed in the other runs.

A DynDom analysis of the extreme conformations reveals the opening and closing domain motions in apo BtuF are characterized by a 56° rotation with residues Ala87, Thr88, Ile90, Glu91, Ser116, Leu117, Ala225, Ser226, and Pro227 acting as hinges. For holo BtuF, no domain motion was detected.

Simulation and X-ray. To relate the simulation results to the available crystal structures, we identified the protein−protein contacts in the apo BtuF crystal (*22*) (Figure 5A), compared the average no-B_{12} structure with the apo crystal structure (Figure 5B), and computed the average radius of gyration for holo and apo BtuF. Additionally, elastic network normal modes were calculated for the apo BtuF crystal structure and the other three group III PBPs for which crystal structures are available (Figure 6).

The distribution of BtuF crystal contacts over the protein's Connolly surface is highlighted in green (Figure 5A). A distance cutoff of 4 Å was used between the protein and its adjacent copies in the unit cell to identify residues involved in crystal contacts. Figure 5B shows the energy-minimized average structure of all no-B_{12} runs superimposed on the apo crystal structure. Structural differences are quantified in a C_α displacement plot where α-helix and *β*-sheet sections are marked with blue rectangles. The two structures are not identical but nevertheless are very similar. Maximum displacements occur in loop regions, and the overall C_α rmsd

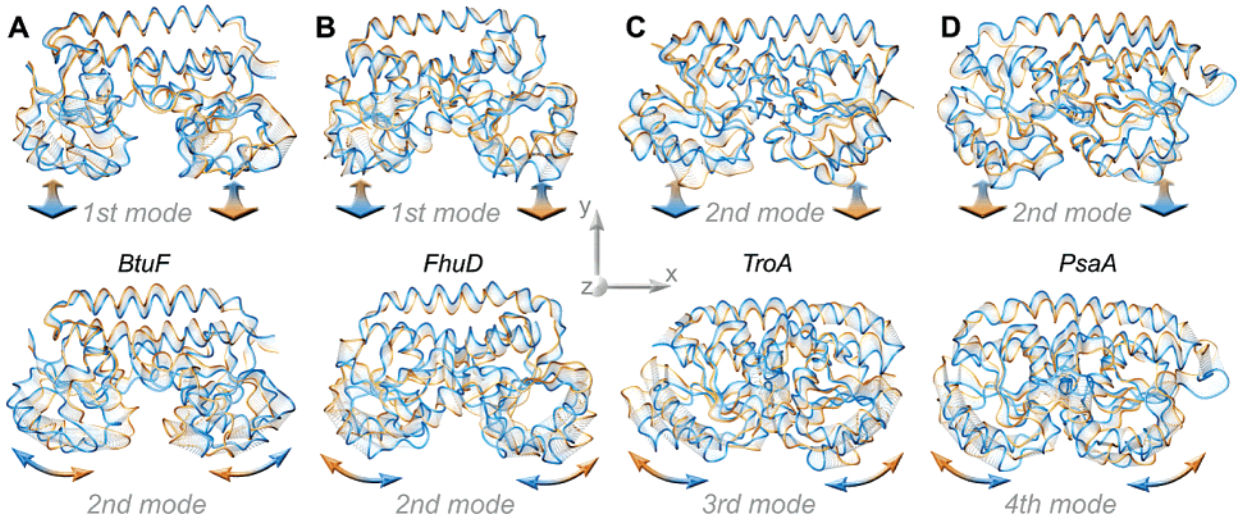

FIGURE 6: Elastic network normal-mode analysis. The opening and closing motions observed in the BtuF simulations are mainly a combination of the first two lowest-frequency modes. The modes describe a converse out-of-plane motion of the domains around the *x*-axis (first mode) and an in-plane opening−closing motion around the *y*-axis (second mode) (A). The same motions are found for the other group III periplasmic binding proteins: FhuD (B), TroA (C), and PsaA (D).

between the no-B_{12} simulation average and the crystal structure is 2.5 Å.

The radius of gyration (R_g) of BtuF was calculated for each trajectory and then averaged to obtain the mean R_g for the apo and holo BtuF. In case of the latter, vitamin B_{12} was included in the calculations. An average R_g of 19.1 ± 0.25 Å was determined for the ligand-free simulations (no-B_{12} and B_{12}-removed), while for the ligand-bound BtuF runs (B_{12}-added and B_{12}-bound), an average R_g of 18.5 ± 0.1 Å was found.

Normal Modes. Elastic network normal-mode analysis on the apo BtuF crystal structure reveals a converse in- and out-of-plane bending motion around the *x*-axis of the N- and C-terminal domains in the first lowest-frequency mode and an opening- and closing-like motion of the two lobes around the out-of-plane *z*-axis in the second lowest-frequency mode (Figure 6A). Together, the two modes provide a good description of the conformational changes observed in the simulations. When elastic network analysis is performed on the three other BtuF-like PBPs, the same kind of bending and opening−closing motions are observed among the first four lowest-frequency modes: the first and second modes in the case of FhuD (Figure 6B), the second and third modes for TroA (Figure 6C), and the second and fourth modes for PsaA (Figure 6D). The other modes (modes 3 and 4 for BtuF and FhuD, modes 1 and 4 for TroA, and modes 1 and 3 for PsaA) describe bending motions around the *y*-axis.

DISCUSSION

Domain Motions. Multicopy molecular dynamics simulations (480 ns) (*32*, *33*) were performed to explore the conformational space accessible to the apo and holo forms of the periplasmic vitamin B_{12} binding protein, BtuF. For each of the four starting structures, three copies were generated, each using a different random distribution of initial velocities leading to different trajectories. This procedure yields an improved sampling of the total conformational space, as reflected by different rmsds produced by the same starting structures (Figure 3). With computer power steadily increasing, multicopy MD simulation will become increasingly more important, as it provides a simple yet effective means of enlarging the sampling rate of conformational space.

Even though protein structure evolves differently in the 12 BtuF trajectories, the root-mean-square deviations of singles domains are always smaller than the corresponding rmsds of the whole protein (Figure 3). However, the rmsd depends not only on the structural similarity between two structures but also on the protein size, being roughly proportional with its radius of gyration (*59*, *60*). Here the difference in domain and total rmsd we observe mainly arises because the N- and C-terminal domains are more stable than the overall protein. This is due to rigid body-like motions of the domains relative to each other. The same pattern has also been observed in the simulation study of apo−holo transitions of maltose binding protein, where structures of both the open and closed states were known as a control on the simulation results (*36*).

The N and C domains move in an opening- and closing-like manner. This is reflected by changes in the C_α distance of conserved glutamates 50 and 180 (Figure 4), which have been proposed to be key residues in the BtuF−BtuC docking interface (*15*, *30*). Opening and closing are observed in both apo and holo simulations, but the motions are larger in the apo runs. Furthermore, in the apo simulations, BtuF tends more toward opening, whereas the holo simulations display a closing trend.

The elastic network normal-mode analysis we performed on BtuF confirms our simulation findings of opening and closing motions: the conformational changes observed in the simulation are described well by a combination of the first two lowest-frequency modes (Figure 6A). As these two independent methods suggest the same conformational changes and we previously obtained accurate results for domain motions in maltose binding protein, we believe it is likely that the opening and closing motions observed in BtuF represent a real section of conformational space accessible to the protein. In addition, it is remarkable that elastic

network analysis yielded very similar results for the other three BtuF-like periplasmic binding proteins for which crystal structures are available. All protein models show comparable out-of-plane bending and opening and closing motions within the first four lowest-frequency normal modes (Figure 6B−D). In case of FhuD, the modes are the same as those for BtuF (first and second), whereas for TroA and PsaA, said motions are found in the second and third modes and second and fourth modes, respectively. The fact that the same motions being described by different normal modes reflects a key limitation of any normal-mode analysis: functionally conformational changes are to be found among the lowest-frequency normal modes, but so far there is no procedure for pinpointing this to particular mode numbers.

Link to Experiment and Previous Simulations of FhuD. Our simulations show that especially apo BtuF is clearly more flexible than previously assumed on grounds of the available X-ray structure (*15*, *22*). A possible explanation for why this has not yet been detected is that crystal packing might hinder conformational changes. This is supported by the distribution of crystal contacts on the surface of the apo protein (Figure 5A). BtuF is capable of opening but is locked in a closed conformation in the protein crystal. On the other hand, crystal contacts are also present in the apo form of maltose binding protein, and here the protein could be trapped in an open conformation even though there is no obvious energetic barrier separating the open and closed state (*61*). However, open maltose binding protein is stabilized by a special interface region on the opposite side of the three-stranded linker region (*60*), that bridges residues of both the N and C terminal domains. This structural feature is apparently not present in BtuF and BtuF-like PBPs due to the α-helical nature of the single domain linker region. It is therefore plausible that the BtuF crystal actually does contain some protein in an open conformation comparable to the ones we observe in our simulation, but the majority of protein conformations present in the crystal represent a closed form. Thus, the open form would remain undetected when the protein structure is determined from such a crystal. The average structure calculated of all apo runs starting from the unmodified no-B_{12} X-ray structure also supports this hypothesis. After energy minimization, the difference between the MD average structure and the X-ray structural model is only small (Figure 5B); the total C_α rmsd is 2.5 Å, and larger deviations occur mainly within loop regions.

Periplasmic binding proteins have also been studied using small-angle X-ray scattering which can be used to determine conformational transitions by measuring the protein's radius of gyration. Although no such study of BtuF has yet been reported, SAXS data on the structurally related FhuD show no change upon ligand binding (*11*, *62*). For maltose binding protein, on the other hand, a difference in the radius of gyration of ∼1 Å was found (*63*). The average radii of gyration computed from all our BtuF simulations in this study yield a difference of 0.6 Å between the apo and holo state (Figure 5C), matching exactly the R_g changes calculated from the apo and holo crystal structures of FhuD and BtuF (*37*). An R_g difference of 0.6 Å is generally interpreted as no significant conformational changes occurring, as indicated by a C_α rmsd of 1.12 Å between the apo and holo BtuF X-ray structures. Furthermore, such a small difference would likely be challenging to resolve experimentally.

MD simulation studies on BtuF have not been previously reported. However, a 30 ns simulation of the related apo FhuD found only a relatively small closing motion, which however already significantly exceeded the scale of motions observed in the X-ray structures (*37*). Although it is possible the large-scale dynamics of the closely related FhuD and BtuF would differ, the different conformational changes observed in the two studies might be only a sampling issue.

Biological Implications. On the basis of our simulation data, BtuF appears to be more flexible than previously assumed from the available X-ray structures. Displaying clear opening and closing motions, BtuF seems to follow the same Venus flytrap mechanism (*8*) that has been postulated for group I and II PBPs. If our simulation results are correct, BtuF does not represent a new functional group but is instead compatible with the second PBP functional model (*10*). In the apo runs, a broad range of wide open and tightly closed conformation is visited (Figure 4C), whereas in the holo simulation, BtuF exhibits a closed conformation with only comparably small fluctuations (Figure 4D). The observed trends to open upon ligand removal (Figure 4A) and to close upon ligand addition (Figure 4B) further support this hypothesis.

Thus, our findings hint at a more general scheme of PBP and ABC transporter interaction: both molecular recognition (empty or loaded PBP) and transporter−binding protein communication seem likely to rely at least partly on domain mobility in the binding protein. In the B_{12} uptake system, the former is likely to involve conserved surface BtuF glutamates and BtuC arginines. A similar mode of interaction between charged residues has also been proposed for the FhuD−FhuB interaction (*37*). A promising candidate for the further investigation of this would be the full BtuCD-F complex whose structural details are still unknown. In our lab, we created possible BtuF−BtuCD docking complexes, and multicopy MD simulations of the systems in a realistic lipid−water environment are currently underway.

Considering both the BtuF simulation results and their remarkable agreement with normal-mode analysis results for all BtuF-like periplasmic binding proteins, we suggest that the Venus flytrap mechanism is likely to apply to other group III periplasmic binding proteins as well. It will be exciting to see this hypothesis investigated further by both theoretical and experimental means such as long-time multicopy MD simulations or double spin-labeled EPR studies like the ones carried out recently on maltose binding protein (*64*).

ACKNOWLEDGMENT

We appreciate discussions on this topic with Drs. H. Vogel, T. Stockner, and M. O'Mara.

REFERENCES

1. Tam, R., and Saier, M. H., Jr. (1993) Structural, functional, and evolutionary relationships among extracellular solute-binding receptors of bacteria, *Microbiol. Rev. 57*, 320−346.
2. Quiocho, F. A., and Ledvina, P. S. (1996) Atomic structure and specificity of bacterial periplasmic receptors for active transport and chemotaxis: Variation of common themes, *Mol. Microbiol. 20*, 17−25.
3. Felder, C. B., Graul, R. C., Lee, A. Y., Merkle, H. P., and Sadee, W. (1999) The Venus flytrap of periplasmic binding proteins: An ancient protein module present in multiple drug receptors, *AAPS PharmSci 1*, E2.

4. Dwyer, M. A., and Hellinga, H. W. (2004) Periplasmic binding proteins: A versatile superfamily for protein engineering, *Curr. Opin. Struct. Biol. 14*, 495−504.
5. Richarme, G., and Caldas, T. D. (1997) Chaperone properties of the bacterial periplasmic substrate-binding proteins, *J. Biol. Chem. 272*, 15607−15612.
6. Koster, W. (2001) ABC transporter-mediated uptake of iron, siderophores, heme and vitamin B12, *Res. Microbiol. 152*, 291−301.
7. Driessen, A. J., Rosen, B. P., and Konings, W. N. (2000) Diversity of transport mechanisms: Common structural principles, *Trends Biochem. Sci. 25*, 397−401.
8. Sack, J. S., Saper, M. A., and Quiocho, F. A. (1989) Periplasmic Binding-Protein Structure and Function: Refined X-ray Structures of the Leucine Isoleucine Valine-Binding Protein and Its Complex with Leucine, *J. Mol. Biol. 206*, 171−191.
9. Newcomer, M. E., Lewis, B. A., and Quiocho, F. A. (1981) The radius of gyration of L-arabinose-binding protein decreases upon binding of ligand, *J. Biol. Chem. 256*, 13218−13222.
10. Oh, B. H., Pandit, J., Kang, C. H., Nikaido, K., Gokcen, S., Ames, G. F., and Kim, S. H. (1993) Three-dimensional structures of the periplasmic lysine/arginine/ornithine-binding protein with and without a ligand, *J. Biol. Chem. 268*, 11348−11355.
11. Clarke, T. E., Tari, L. W., and Vogel, H. J. (2001) Structural biology of bacterial iron uptake systems, *Curr. Top. Med. Chem. 1*, 7−30.
12. Newcomer, M. E., Gilliland, G. L., and Quiocho, F. A. (1981) L-Arabinose-binding protein-sugar complex at 2.4 Å resolution. Stereochemistry and evidence for a structural change, *J. Biol. Chem. 256*, 13213−13217.
13. Spurlino, J. C., Lu, G. Y., and Quiocho, F. A. (1991) The 2.3-Å resolution structure of the maltose- or maltodextrin-binding protein, a primary receptor of bacterial active transport and chemotaxis, *J. Biol. Chem. 266*, 5202−5219.
14. Fukami-Kobayashi, K., Tateno, Y., and Nishikawa, K. (1999) Domain dislocation: A change of core structure in periplasmic binding proteins in their evolutionary history, *J. Mol. Biol. 286*, 279−290.
15. Borths, E. L., Locher, K. P., Lee, A. T., and Rees, D. C. (2002) The structure of *Escherichia coli* BtuF and binding to its cognate ATP binding cassette transporter, *Proc. Natl. Acad. Sci. U.S.A. 99*, 16642−16647.
16. Sharff, A. J., Rodseth, L. E., Spurlino, J. C., and Quiocho, F. A. (1992) Crystallographic Evidence of a Large Ligand-Induced Hinge-Twist Motion between the 2 Domains of the Maltodextrin Binding-Protein Involved in Active-Transport and Chemotaxis, *Biochemistry 31*, 10657−10663.
17. Lee, Y. H., Deka, R. K., Norgard, M. V., Radolf, J. D., and Hasemann, C. A. (1999) *Treponema pallidum* TroA is a periplasmic zinc-binding protein with a helical backbone, *Nat. Struct. Biol. 6*, 628−633.
18. Lee, Y. H., Dorwart, M. R., Hazlett, K. R., Deka, R. K., Norgard, M. V., Radolf, J. D., and Hasemann, C. A. (2002) The crystal structure of Zn(II)-free *Treponema pallidum* TroA, a periplasmic metal-binding protein, reveals a closed conformation, *J. Bacteriol. 184*, 2300−2304.
19. Lawrence, M. C., Pilling, P. A., Epa, V. C., Berry, A. M., Ogunniyi, A. D., and Paton, J. C. (1998) The crystal structure of pneumococcal surface antigen PsaA reveals a metal-binding site and a novel structure for a putative ABC-type binding protein, *Structure 6*, 1553−1561.
20. Clarke, T. E., Ku, S. Y., Dougan, D. R., Vogel, H. J., and Tari, L. W. (2000) The structure of the ferric siderophore binding protein FhuD complexed with gallichrome, *Nat. Struct. Biol. 7*, 287−291.
21. Krewulak, K. D. (2005) Bacterial Periplasmic Siderophore Binding Proteins, Ph.D. Thesis, University of Calgary, Calgary, AB.
22. Karpowich, N. K., Huang, H. H., Smith, P. C., and Hunt, J. F. (2003) Crystal structures of the BtuF periplasmic-binding protein for vitamin B12 suggest a functionally important reduction in protein mobility upon ligand binding, *J. Biol. Chem. 278*, 8429−8434.
23. Cadieux, N., Bradbeer, C., Reeger-Schneider, E., Koster, W., Mohanty, A. K., Wiener, M. C., and Kadner, R. J. (2002) Identification of the periplasmic cobalamin-binding protein BtuF of *Escherichia coli*, *J. Bacteriol. 184*, 706−717.
24. Chimento, D. P., Mohanty, A. K., Kadner, R. J., and Wiener, M. C. (2003) Substrate-induced transmembrane signaling in the cobalamin transporter BtuB, *Nat. Struct. Biol. 10*, 394−401.
25. Locher, K. P., Lee, A. T., and Rees, D. C. (2002) The *E. coli* BtuCD structure: A framework for ABC transporter architecture and mechanism, *Science 296*, 1091−1098.
26. Davidson, A. L., and Chen, J. (2004) ATP-binding cassette transporters in bacteria, *Annu. Rev. Biochem. 73*, 241−268.
27. Chang, G., and Roth, C. B. (2001) Structure of MsbA from *E. coli*: A homolog of the multidrug resistance ATP binding cassette (ABC) transporters, *Science 293*, 1793−1800.
28. Chang, G. (2003) Structure of MsbA from *Vibrio cholera*: A multidrug resistance ABC transporter homolog in a closed conformation, *J. Mol. Biol. 330*, 419−430.
29. Reyes, C. L., and Chang, G. (2005) Structure of the ABC transporter MsbA in complex with ADP•vanadate and lipopolysaccharide, *Science 308*, 1028−1031.
30. Locher, K. P., and Borths, E. (2004) ABC transporter architecture and mechanism: Implications from the crystal structures of BtuCD and BtuF, *FEBS Lett. 564*, 264−268.
31. Borths, E. L., Poolman, B., Hvorup, R. N., Locher, K. P., and Rees, D. C. (2005) In vitro functional characterization of BtuCD-F, the *Escherichia coli* ABC transporter for vitamin B-12 uptake, *Biochemistry 44*, 16301−16309.
32. Caves, L. S., Evanseck, J. D., and Karplus, M. (1998) Locally accessible conformations of proteins: Multiple molecular dynamics simulations of crambin, *Protein Sci. 7*, 649−666.
33. Das, B., Helms, V., Lounnas, V., and Wade, R. C. (2000) Multicopy molecular dynamics simulations suggest how to reconcile crystallographic and product formation data for camphor enantiomers bound to cytochrome P-450cam, *J. Inorg. Biochem. 81*, 121−131.
34. Pang, A., Arinaminpathy, Y., Sansom, M. S. P., and Biggin, P. C. (2003) Interdomain dynamics and ligand binding: Molecular dynamics simulations of glutamine binding protein, *FEBS Lett. 550*, 168−174.
35. Arinaminpathy, Y., Sansom, M. S., and Biggin, P. C. (2002) Molecular dynamics simulations of the ligand-binding domain of the ionotropic glutamate receptor GluR2, *Biophys. J. 82*, 676−683.
36. Stockner, T., Vogel, H. J., and Tieleman, D. P. (2005) A salt-bridge motif involved in ligand binding and large-scale domain motions of the maltose-binding protein, *Biophys. J. 89*, 3362−3371.
37. Krewulak, K. D., Shepherd, C. M., and Vogel, H. J. (2005) Molecular dynamics simulations of the periplasmic ferric-hydroxamate binding protein FhuD, *BioMetals 18*, 375−386.
38. Lindahl, E., and Delarue, M. (2005) Refinement of docked protein−ligand and protein-DNA structures using low-frequency normal mode amplitude optimization, *Nucleic Acids Res. 33*, 4496−4506.
39. Tama, F., and Sanejouand, Y. H. (2001) Conformational change of proteins arising from normal mode calculations, *Protein Eng. 14*, 1−6.
40. Valadie, H., Lacapcre, J. J., Sanejouand, Y. H., and Etchebest, C. (2003) Dynamical properties of the MscL of *Escherichia coli*: A normal-mode analysis, *J. Mol. Biol. 332*, 657−674.
41. Chacon, P., Tama, F., and Wriggers, W. (2003) Mega-Dalton biomolecular motion captured from electron microscopy reconstructions, *J. Mol. Biol. 326*, 485−492.
42. Tama, F., Valle, M., Frank, J., and Brooks, C. L., III (2003) Dynamic reorganization of the functionally active ribosome explored by normal mode analysis and cryo-electron microscopy, *Proc. Natl. Acad. Sci. U.S.A. 100*, 9319−9323.
43. Berendsen, H. J. C., Vanderspoel, D., and Vandrunen, R. (1995) Gromacs: A Message-Passing Parallel Molecular-Dynamics Implementation, *Comput. Phys. Commun. 91*, 43−56.
44. Lindahl, E., Hess, B., and van der Spoel, D. (2001) GROMACS 3.0: A package for molecular simulation and trajectory analysis, *J. Mol. Model. 7*, 306−317.
45. Berendsen, H. J. C., Postma, J. P. M., Vangunsteren, W. F., and Hermans, J. (1981) Interaction models for water in relation to protein hydration, in *Intermolecular Forces* (Pullman, B., Ed.) pp 331−342, Reidel, Dordrecht, The Netherlands.
46. Berendsen, H. J. C., Postma, J. P. M., Vangunsteren, W. F., Dinola, A., and Haak, J. R. (1984) Molecular-Dynamics with Coupling to an External Bath, *J. Chem. Phys. 81*, 3684−3690.
47. Darden, T., York, D., and Pedersen, L. (1993) Particle Mesh Ewald: An N.Log(N) Method for Ewald Sums in Large Systems, *J. Chem. Phys. 98*, 10089−10092.

48. Essmann, U., Perera, L., Berkowitz, M. L., Darden, T., Lee, H., and Pedersen, L. G. (1995) A Smooth Particle Mesh Ewald Method, *J. Chem. Phys. 103*, 8577−8593.
49. Marques, H. M., Ngoma, B., Egan, T. J., and Brown, K. L. (2001) Parameters for the AMBER force field for the molecular mechanics modeling of the cobalt corrinoids, *J. Mol. Struct. 561*, 71−91.
50. Marques, H. M., and Brown, K. L. (1995) A Molecular Mechanics Force-Field for the Cobalt Corrinoids, *THEOCHEM 340*, 97−124.
51. Frisch, M. J., Trucks, G. W., Schlegel, H. B., Scuseria, G. E., Robb, M. A., Cheeseman, J. R., Montgomery, J. A., Jr., Vreven, T., Kudin, K. N., Burant, J. C., Millam, J. M., Iyengar, S. S., Tomasi, J., Barone, V., Mennucci, B., Cossi, M., Scalmani, G., Rega, N., Petersson, G. A., Nakatsuji, H., Hada, M., Ehara, M., Toyota, K., Fukuda, R., Hasegawa, J., Ishida, M., Nakajima, T., Honda, Y., Kitao, O., Nakai, H., Klene, M., Li, X., Knox, J. E., Hratchian, H. P., Cross, J. B., Bakken, V., Adamo, C., Jaramillo, J., Gomperts, R., Stratmann, R. E., Yazyev, O., Austin, A. J., Cammi, R., Pomelli, C., Ochterski, J. W., Ayala, P. Y., Morokuma, K., Voth, G. A., Salvador, P., Dannenberg, J. J., Zakrzewski, V. G., Dapprich, S., Daniels, A. D., Strain, M. C., Farkas, O., Malick, D. K., Rabuck, A. D., Raghavachari, K., Foresman, J. B., Ortiz, J. V., Cui, Q., Baboul, A. G., Clifford, S., Cioslowski, J., Stefanov, B. B., Liu, G., Liashenko, A., Piskorz, P., Komaromi, I., Martin, R. L., Fox, D. J., Keith, T., Al-Laham, M. A., Peng, C. Y., Nanayakkara, A., Challacombe, M., Gill, P. M. W., Johnson, B., Chen, W., Wong, M. W., Gonzalez, C., and Pople, J. A. (2004) *Gaussian 03*, revision C.02, Gaussian Inc., Wallingford, CT.
52. Becke, A. D. (1993) Density-Functional Thermochemistry. 3. The Role of Exact Exchange, *J. Chem. Phys. 98*, 5648−5652.
53. Lee, C. T., Yang, W. T., and Parr, R. G. (1988) Development of the Colle-Salvetti Correlation-Energy Formula into a Functional of the Electron-Density, *Phys. Rev. B 37*, 785−789.
54. Hay, P. J., and Wadt, W. R. (1985) Abinitio Effective Core Potentials for Molecular Calculations: Potentials for the Transition-Metal Atoms Sc to Hg, *J. Chem. Phys. 82*, 270−283.
55. Reed, A. E., Weinstock, R. B., and Weinhold, F. (1985) Natural-Population Analysis, *J. Chem. Phys. 83*, 735−746.
56. Hayward, S., Kitao, A., and Berendsen, H. J. (1997) Model-free methods of analyzing domain motions in proteins from simulation: A comparison of normal mode analysis and molecular dynamics simulation of lysozyme, *Proteins 27*, 425−437.
57. Hayward, S., and Berendsen, H. J. (1998) Systematic analysis of domain motions in proteins from conformational change: New results on citrate synthase and T4 lysozyme, *Proteins 30*, 144−154.
58. Hayward, S., and Lee, R. A. (2002) Improvements in the analysis of domain motions in proteins from conformational change: DynDom version 1.50, *J. Mol. Graphics Modell. 21*, 181−183.
59. Reva, B. A., Finkelstein, A. V., and Skolnick, J. (1998) What is the probability of a chance prediction of a protein structure with an rmsd of 6 A? *Folding Des. 3*, 141−147.
60. Betancourt, M. R., and Skolnick, J. (2001) Universal similarity measure for comparing protein structures, *Biopolymers 59*, 305−309.
61. Telmer, P. G., and Shilton, B. H. (2003) Insights into the conformational equilibria of maltose-binding protein by analysis of high affinity mutants, *J. Biol. Chem. 278*, 34555−34567.
62. Sebulsky, M. T., Shilton, B. H., Speziali, C. D., and Heinrichs, D. E. (2003) The role of FhuD2 in iron(III)-hydroxamate transport in *Staphylococcus aureus*. Demonstration that FhuD2 binds iron(III)-hydroxamates but with minimal conformational change and implication of mutations on transport, *J. Biol. Chem. 278*, 49890−49900.
63. Shilton, B. H., Flocco, M. M., Nilsson, M., and Mowbray, S. L. (1996) Conformational changes of three periplasmic receptors for bacterial chemotaxis and transport: The maltose-, glucose/galactose- and ribose-binding proteins, *J. Mol. Biol. 264*, 350−363.
64. Austermuhle, M. I., Hall, J. A., Klug, C. S., and Davidson, A. L. (2004) Maltose-binding protein is open in the catalytic transition state for ATP hydrolysis during maltose transport, *J. Biol. Chem. 279*, 28243−28250.
65. Hess, B., Bekker, H., Berendsen, H. J. C., Fraaije, J. G. E. M. (1997) LINCS: A linear constraint solver for molecular simulations, *J. Compot. Chem. 18*, 1463−1472.

BI061280J